Model-based state of charge estimation algorithms under various current patterns

Available online at www.sciencedirect.com

ScienceDirect

Energy Procedia 158 (2019) 2806–2811

Energy Procedia

www.elsevier.com/locate/procedia

10th International Conference on Applied Energy (ICAE2018), 22-25 August 2018, Hong Kong, China

Model-based state of charge estimation algorithms under various current patterns

Shi Li[a] *, Changfu Zou[b], Mirco Küpper[c], Stefan Pischinger[a]

[a]*Institute for Combustion Engines, RWTH Aachen University, Forckenbeckstrasse 4, D-52074 Aachen, Germany*
[b]*Department of Electrical Engineering, Chalmers University of Technology, Gothenburg 41296, Sweden*
[c]*FEV Europe GmbH, Neuenhofstrasse 181, D-52078 Aachen, Germany*

Abstract

Numerous model-based techniques have been proposed to estimate the state of charge (SOC) of lithium-ion batteries. In automotive applications, the algorithms are subjected to changing load profiles, requiring investigations into their general performance under various working conditions. In this study, three different load patterns derived from a customized dynamic driving profile, a standard driving cycle, and a constant discharge are used for the experimental verification. Four selected algorithms including the Ampere-hour counting, the extended Kalman filter, the particle filter, and the recursive least square filter are implemented. Their performance in terms of accuracy and robustness are compared. In addition, the load profile is analyzed in the frequency domain. The results show that the filter performance is dependent on the current patterns and can be correlated to the frequency spectrum of the load profile.

Keywords: Electric vehicles; State of charge; Load condition; Extended Kalman filter; Particle filter; Recursive least square

1. Introduction

The model-based algorithm is the most widely investigated technique for state of charge (SOC) estimation of lithium-ion batteries. The main idea of the model-based SOC estimation is to establish the relationship between the

* Corresponding author. Tel.: +49-241-80 48244; fax: +49-241-80 92630.
E-mail address: Li_shi@vka.rwth-aachen.de

1876-6102
10.1016/j.egypro.2019.02.042

measured signals (current, voltage, and temperature) and the SOC by using a battery model. The model can be connected to the cell measurement by employing a filter algorithm from modern control theory to form a closed-loop estimation system. In these systems, the residual between the modeled and measured battery output is used for the correction of the estimated states. In this way, inaccuracy caused by battery models and measured signals can be reduced. The most widely used filtering algorithm is Kalman filter (KF). The standard Kalman filter is only suitable for linear systems. So it can be applied to simple models [1,2]. When the system is nonlinear (like battery models), more advanced variants of Kalman filter should be used. Extended Kalman filter (EKF) is used for SOC estimation in [3–9], and Sigma-point Kalman filter (SPKF) is applied in [10–12]. Kalman filter and its variants assume that all uncertainties and noises have zero mean and Gaussian distribution. Adaptive Kalman filter (AKF) and its variations [13–15] are applied to estimate the model and measurement noises online. To overcome the limit brought by the Gaussian assumption, particle filter (PF) or Monte Carlo filter is employed in [16–18] for SOC estimation. KF, PF, and their variations belong to Bayesian filters known in control theory. The recursive least squares (RLS) filters with an optimal forgetting factor is used to estimate SOC in [19–21]. Furthermore, other observers and controllers are also used for SOC estimation, for example, the sliding mode observer and the Luenberger observer [22,23].

Although a variety of methods are presented above, they are usually only validated with a single load pattern. Few have tackled the difference of the algorithms in different working conditions. In this study, a second-order equivalent circuit model is built for a Lithium-Nickel-Manganese-Cobalt-Oxide (LiNMC) high-energy pouch cell with the parameters derived from the pulse test. Four representative algorithms including Ah counting, EKF, PF, and RLS are implemented. And an evaluation and comparison among them are performed. Furthermore, Fourier transformation is used to analyze the frequency characteristics of load profiles. Conclusions are drawn regarding the filter performance and the correlation to load profiles.

The remainder of this paper is organized as follows: in Section 2, the implementation of algorithm and model are briefly explained; in Section 3, the test conditions, i.e., applied current patterns and synthetic errors are described; in Section 3, the performances of SOC estimation under respective working condition are compared and analyzed. The conclusions are drawn in Section 4.

2. Model and algorithm implementations

The model structure is the equivalent circuit model with one voltage source for open circuit voltage (OCV), one resistance for internal resistance, and two parallel connected resistance-capacitance (RC) networks. The parameterization test is the ten-second pulse test according to the standard IEC 62660-1. More details regarding the experiment can be found in [24]. The nonlinear least square method is used to fit the model response to the measured curves. The objective function for fitting is:

$$e = \sqrt{\frac{1}{t_2 - t_1}\int_{t_1}^{t_2}\left[U_{sim}(t) - U_{mea}(t)\right]^2 dt} \tag{1}$$

where U_{mea} is the measured voltage from the test, and U_{sim} the simulated voltage from the model. The optimization process is repeated to minimize the objective function. The voltage response of the 2-RC model in pulse and relaxation periods can be calculated by:

$$U_{sim}(t) = U_{OCV} + Factor \cdot \left[R_o \cdot I_{pulse} + \sum_{i=1}^{2} R_i \cdot I_{pulse} \cdot (1 - \exp(-\frac{t}{R_i \cdot C_i})) \right] + (1 - Factor) \cdot \left[\sum_{i=1}^{2} \tilde{U}_i \cdot (\exp(-\frac{t}{R_i \cdot C_i})) \right] \tag{2}$$

where the second term on the right side of (2) is the voltage during the pulse period, and the third term the voltage during the relaxation period. *Factor* is a variable to differentiate the pulse and relax periods, which is set to 1 during the pulse and 0 during relaxation. $\tilde{U}_i$ represents the initial voltage of the i^{th} RC for the relaxation period, where i equals 1 or 2.

The tested algorithms are three popular model-based algorithms (EKF, PF, and RLS). The traditional Ampere-hour counting approach (Ah) is also used as a reference. For the detailed implementation procedures, the readers are kindly referred to the papers mentioned in Section 1.

3. Verification conditions

The validation tests to gather data are carried out on the LiNMC cell. It is essential to know the general performance of the algorithms instead of a specific working condition. Therefore, three different load profiles with different durations and different current patterns are applied in the validation tests. The current profiles and their voltage responses are shown in Fig. 1. The working condition (a) is derived from a customized dynamic profile used for electric vehicle testing. The cell is fully charged and then discharged to around 70%. The working condition (b) is derived from a standard driving cycle called Artemis Urban. The cell is initialized with 68% and discharged to 63%. The working condition (c) is to evaluate the performance under a static load. The cell is fully charged and then discharged with 1/3 C for 5000s.

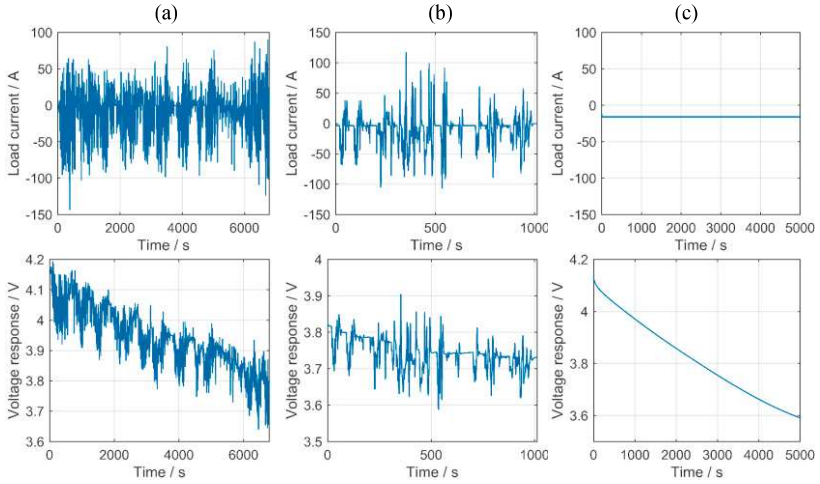

Fig. 1. Current profile and corresponding voltage response of the validation measurement (a), (b), and (c)

The sensor noises must be considered to simulate the vehicle application. Both Gaussian noise and non-Gaussian noise need to be considered. The synthetic sensor noise is approximated according to state-of-the-art sensor suppliers. For the current sensor, the offset is set to 25 mA, the gain error 0.3%, and the covariance of the white noise 2 mA. For the voltage sensor, the offset is set to 6 mV, and the covariance of the white noise 10 mV.

4. Results and analysis

In the following, the estimation accuracy and convergence behavior are evaluated. The tested algorithms are the traditional Ampere-hour counting approach (Ah) and three popular model-based algorithms (EKF, PF, and RLS). The parameterizations of the filters have a direct impact on the performance. They are usually determined based on the knowledge of model and sensor accuracy. In addition, some tuning for practical situations might be necessary. For the sake of comparison, the tuning in this work is conducted in a way that the filters have very close accuracy in the first validation test. Then the parameters are kept the same for the rest of verifications. The number of particles in PF will also influence the accuracy and adaptability of this algorithm. But more particles used will increase the computational burden of the filter. Therefore, the particle number has to be chosen considering these aspects. It is fixed to 100 in this study.

To examine the accuracy of the four algorithms, they are initialized correctly. The SOC calculated using the correct current is taking as the reference SOC. The simulation results of estimation error are plotted in Fig. 2. An overview of results at different working conditions is listed in Table 1.

Compared with three model-based algorithms, the estimation with Ah counting displays the best accuracy. This is due to the fact that nowadays the commercially available sensors already have high accuracies. When the initialization is correct, the estimation accuracy is mainly influenced by the sensor accuracy and time. The estimation error of Ah displays an increasing trend owing to the nature of integration calculation. The error due to imperfect measurements will accumulate and becomes critical for long-term performance.

The root-mean-square errors (RMSE) of three model-based algorithms are very close in working condition (a). This is due to the fact that the filters are tuned based on this working condition. This is taken as an equal starting point for the comparison. Although the RMSEs are close, PF and EKF display similar curves, which are distinctly different from RLS.

The three filters behave differently in different working conditions. EKF has the smallest maximum error in (a), RLS the smallest in (b), and PF the smallest in (c). Comparing the two Bayesian filters, PF is worse in (b) and better in (c). Clearly, the filter performance is working condition dependent. The worst case is the (c) with the constant current.

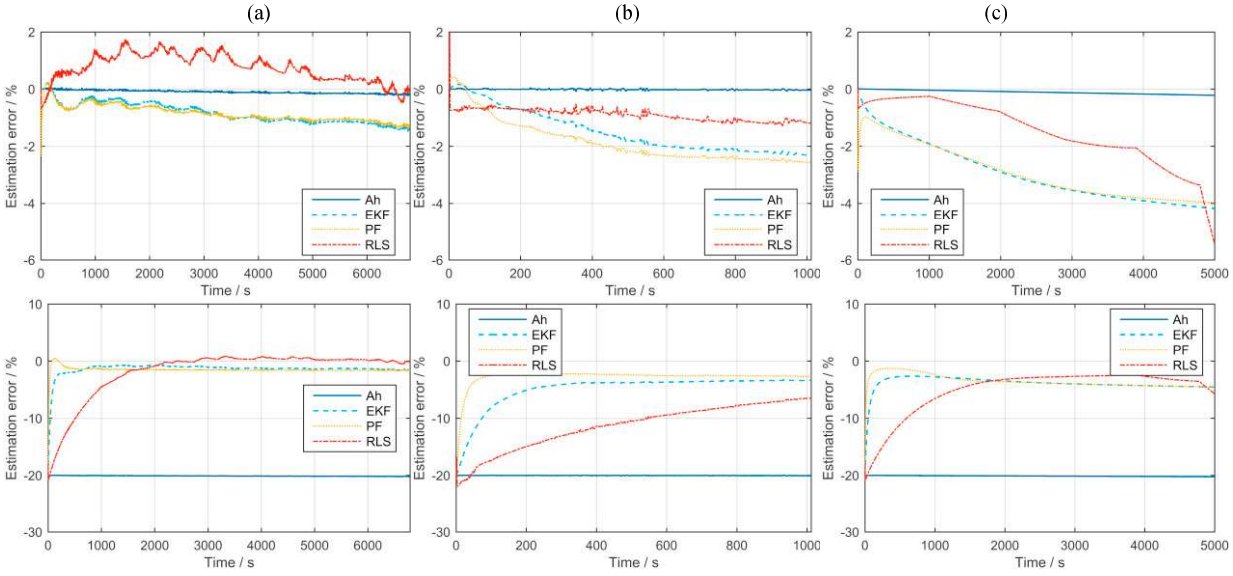

Fig. 2. Estimation results of algorithms for load conditions (a), (b), and (c), correct initialization (above) and incorrect initialization (below)

Table 1. Comparison of different algorithms.

	Load condition (a)				Load condition (b)				Load condition (c)			
Correct initialization												
	Ah	EKF	PF	RLS	Ah	EKF	PF	RLS	Ah	EKF	PF	RLS
RMSE (%)	0.11	0.90	0.90	0.90	0.02	1.65	1.98	0.92	0.12	3.12	3.07	1.86
Maximum (%)	0.25	1.49	2.33	1.76	0.08	2.31	2.56	2.10	0.21	4.17	3.96	5.46
Incorrect initialization												
RMSE (%)	20.09	1.80	1.62	4.62	20.01	5.71	3.19	11.99	20.10	4.03	3.67	6.41
Convergence time (s)	n/a	139	33	1282	n/a	n/a	69	n/a	n/a	330	56	2169

To examine the robustness of the four algorithms, they are initialized with SOCs which are 20% lower than their correct values. The estimation results are plotted in Fig. 2. When the output of the algorithm reaches 3% error bound of the SOC reference value, the estimation is considered converged. The time from the initialization until this stage, called convergence time, is used to quantify the convergence speed. The RMSE and the convergence time are summarized in Table 1.

The Ah method is expected to have no robustness against erroneous initialization. Among the three model-based algorithms, the difference in convergence speed is evident. As shown in the figures, PF is the fastest and RLS the slowest. Due to the fastest convergence speed, PF always displays the best RMSE.

As next, the frequencies in the power signal of the validation profile are determined using discrete Fourier transformation. The x-axis represents the different excitation frequencies. The y-axis is the relative power spectrum density. Frequencies with higher power density will play a more critical role in the estimation results than those with lower density. As the absolute power densities for the three spectra differ significantly in magnitude, they are divided by their maximum value respectively for a better comparison.

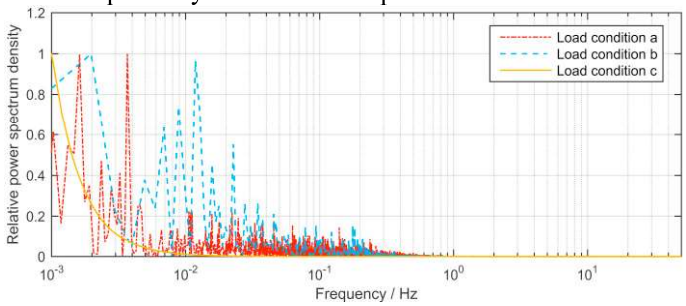

Fig. 3. The frequency spectra of three load conditions

Fig. 3 shows the frequency spectrum of three investigated load profiles from Section 3. All three profiles are measured at a sampling rate of 100Hz. According to Nyquist-Shannon sampling theorem, the highest possible frequency that can be represented in this spectrum is 50Hz. However, all excitation frequencies in the driving profiles are below 10Hz.

The second load condition is derived from Artemis Urban driving cycle. It aims to describe the typical driving condition in the city. Therefore, it has lower dynamic load and less high-frequency content compared to load condition (a). The third condition is the constant discharge. It has the extreme situation that only low frequency exists. With more low-frequency portion in the load pattern, less excitation can be provided to the battery model. This might explain the difference of accuracy for all three model-based algorithms in the previous comparison.

5. Conclusions

In this paper, four popular algorithms for SOC estimation are implemented and examined. Three different load profiles are used. The gain and offset errors are considered. The validation tests have illustrated that the filter performance and their superiority over each other are dependent on the working conditions. A general conclusion on superiority among the three filter algorithms should thus not be drawn merely. Among the three load profiles, the accuracy of the filters increases when the amplitude of the low-frequency in the spectra decreases. The working condition of the constant current is the most difficult for all filter algorithms to predict. As electric vehicles are applied under various dynamic conditions, the adaptability and generality of SOC algorithms should be handled carefully. Further investigations are required to obtain a more accurate relationship between the load frequency and filter performance.

Acknowledgements

This research is supported by research partnership ‘‘ANFAHRT’’ between the RWTH Aachen University and the University of Applied Sciences FH Aachen. It is funded by Ministerium für Innovation, Wissenschaft und Forschung des Landes Nordrhein-Westfalen (MIWFT NRW). FEV GmbH is the industrial partner.

References

[1] Yan J, Li C, Xu G, Xu Y. A novel on-line self-learning state-of-charge estimation of battery management system for hybrid electric

vehicle. IEEE Intell Veh Symp Proc 2009:1161–6. doi:10.1109/IVS.2009.5164446.

[2] Cheng KWE, Divakar BP, Wu H, Ding K, Ho HF. Battery-management system (BMS) and SOC development for electrical vehicles. IEEE Trans Veh Technol 2011;60:76–88. doi:10.1109/TVT.2010.2089647.

[3] Plett GL. Extended Kalman filtering for battery management systems of LiPB-based HEV battery packs Part 1. Background. J Power Sources 2004;134:252–61. doi:10.1016/j.jpowsour.2004.02.031.

[4] Dai H, Wei X, Sun Z, Wang J, Gu W. Online cell SOC estimation of Li-ion battery packs using a dual time-scale Kalman filtering for EV applications. Appl Energy 2012;95:227–37. doi:10.1016/j.apenergy.2012.02.044.

[5] Hu X, Li S, Peng H, Sun F. Robustness analysis of State-of-Charge estimation methods for two types of Li-ion batteries. J Power Sources 2012;217:209–19. doi:10.1016/j.jpowsour.2012.06.005.

[6] Hu C, Youn BD, Chung J. A multiscale framework with extended Kalman filter for lithium-ion battery SOC and capacity estimation. Appl Energy 2012;92:694–704. doi:10.1016/j.apenergy.2011.08.002.

[7] Kim J, Cho BH. State-of-charge estimation and state-of-health prediction of a Li-Ion degraded battery based on an EKF combined with a per-unit system. IEEE Trans Veh Technol 2011;60:4249–60. doi:10.1109/TVT.2011.2168987.

[8] Lee J, Nam O, Cho BH. Li-ion battery SOC estimation method based on the reduced order extended Kalman filtering. J Power Sources 2007;174:9–15. doi:10.1016/j.jpowsour.2007.03.072.

[9] Zou C, Manzie C, Nesic D, Kallapur AG. Multi-time-scale observer design for state-of-charge and state-of-health of a lithium-ion battery. J Power Sources 2016;335:121–30. doi:10.1016/j.jpowsour.2016.10.040.

[10] Plett GL. Sigma-point Kalman filtering for battery management systems of LiPB-based HEV battery packs Part 1: Introduction and state estimation. J Power Sources 2006;161:1356–68. doi:10.1016/j.jpowsour.2006.06.003.

[11] Li J, Barillas JK, Guenther C, Danzer MA. A comparative study of state of charge estimation algorithms for LiFePO 4 batteries used in electric vehicles. J Power Sources 2013;230:244–50. doi:10.1016/j.jpowsour.2012.12.057.

[12] Wang L, Wang L, Liao C, Liu J. Sigma-point Kalman filter application on estimating battery SOC. 5th IEEE Veh Power Propuls Conf VPPC '09 2009:1592–5. doi:10.1109/VPPC.2009.5289604.

[13] Sepasi S, Ghorbani R, Liaw BY. SOC estimation for aged lithium-ion batteries using model adaptive extended Kalman filter. 2013 IEEE Transp Electrif Conf Expo 2013:1–6. doi:10.1109/ITEC.2013.6573479.

[14] Michel P-H, Heiries V. An Adaptive Sigma Point Kalman Filter Hybridized by Support Vector Machine Algorithm for Battery SoC and SoH Estimation. 2015 IEEE 81st Veh. Technol. Conf. (VTC Spring), vol. 2015, IEEE; 2015, p. 1–7. doi:10.1109/VTCSpring.2015.7145678.

[15] Xiong R, He H, Sun F, Zhao K. Evaluation on State of Charge Estimation of Batteries With Adaptive Extended Kalman Filter by Experiment Approach. IEEE Trans Veh Technol 2013;62:108–17. doi:10.1109/TVT.2012.2222684.

[16] Zahid T, Xu G, Li W, Zhao L, Xu K. Performance Analysis of Particle Filter for SOC Estimation of LiFePO4 Battery Pack for Electric Vehicles. Proc IEEE Int Conf Inf Autom 2014:1061–5.

[17] Schwunk S, Armbruster N, Straub S, Kehl J, Vetter M. Particle filter for state of charge and state of health estimation for lithium-iron phosphate batteries. J Power Sources 2013;239:705–10. doi:10.1016/j.jpowsour.2012.10.058.

[18] Hao X, Wu J. Online State Estimation Using Particles Filters of Lithium-Ion Polymer Battery Packs for Electric Vehicle. 2015 IEEE Int. Conf. Syst. Man, Cybern., IEEE; 2015, p. 783–8. doi:10.1109/SMC.2015.146.

[19] Hu X, Sun F, Zou Y, Peng H. Online estimation of an electric vehicle Lithium-Ion battery using recursive least squares with forgetting. Proc 2011 Am Control Conf 2011:935–40. doi:10.1109/ACC.2011.5991260.

[20] Xiong R, He H, Sun F, Zhao K. Online estimation of peak power capability of Li-Ion batteries in electric vehicles by a hardware-in-loop approach. Energies 2012;5:1455–69. doi:10.3390/en5051455.

[21] He H, Zhang X, Xiong R, Xu Y, Guo H. Online model-based estimation of state-of-charge and open-circuit voltage of lithium-ion batteries in electric vehicles. Energy 2012;39:310–8. doi:10.1016/j.energy.2012.01.009.

[22] Chen X, Shen W, Cao Z, Kapoor A. Sliding mode observer for state of charge estimation based on battery equivalent circuit in electric vehicles. Aust J Electr Electron Eng 2012;9:601–6. doi:10.7158/E11-056.2012.9.3.

[23] Tang X, Liu B, Lv Z, Gao F. Observer based battery SOC estimation: Using multi-gain-switching approach. Appl Energy 2017;204:1275–83. doi:10.1016/j.apenergy.2017.03.079.

[24] Li S, Pischinger S, He C, Liang L, Stapelbroek M. A comparative study of model-based capacity estimation algorithms in dual estimation frameworks for lithium-ion batteries under an accelerated aging test. Appl Energy 2018;212:1522–36. doi:10.1016/j.apenergy.2018.01.008.